

Numerical Investigation of the Effects of Bumps on Inflatable Wing Profiles

Daniel A. Reasor Jr.*; Raymond P. LeBeau Jr.†

Dept. of Mechanical Engineering, University of Kentucky, Lexington, KY 40506, U.S.A

This paper discusses results from two dimensional simulations of a “smooth” Eppler 398 wing profile and an inflatable or “bumpy” Eppler 398 wing profile. A discussion on computed flowfields follows for a number of test cases in an effort to understand the unique behavior seen in wind tunnel tests of inflatable wings. Numerical and experimental observations suggest that the flow over the “bumpy” profile has less separation than that of the “smooth” profile for the low Reynolds number cases studied. Both studies also suggest that the flow over the “bumpy” airfoil is more unsteady than that over the “smooth” airfoil.

Nomenclature

α	=	angle of attack	p^*	=	dimensionless pressure
c	=	chord length	t	=	time
Re	=	Reynolds number based on chord length	t^*	=	dimensionless time
C_d	=	drag coefficient	U_∞	=	free-stream velocity
C_l	=	lift coefficient	u^*	=	dimensionless x velocity
C_p	=	pressure coefficient	x^*	=	dimensionless x coordinate
p	=	static pressure	y^*	=	dimensionless y coordinate

I. Introduction

CURRENT research involving lightweight UAVs includes investigations into uses of inflatable wings.¹ Uses for lightweight UAVs include surveillance for homeland security, military applications, and exploration in conditions in the higher altitudes of earth similar to that of other planets such as Mars.²⁻⁵ These inflatable wings inherently possess bumps which modify their baseline profile. The manufacturing techniques used to construct them create their bumpy profile. Not only do inflatable wings possess the ability to be packaged in a relatively small space,⁶ they have the ability to implement wing warping technology as a method of roll control.⁷ Furthermore, these lightweight UAVs fly in regimes where Reynolds numbers are on the $\mathcal{O}10,000$.⁸

One of the problems that is inherent to flight at low Reynolds numbers is the formation of the separation bubble on the upper surface which is due to an adverse pressure gradient. After the separation bubble forms, the pressure tries to recover past half chord of the airfoil. In doing so, the laminar boundary layer tends to separate from the surface. This separation is the source for the large increases in pressure drag. Depending on the specific configuration, the flow can continue to evolve into a number of different possibilities. In some instances it can reattach and form a turbulent boundary layer and in other cases the boundary layer remains unattached.⁹ For smooth airfoils, it has been shown that there is a critical Reynolds number of $\approx 70,000$ for which the boundary layer can reattach. If the Reynolds number is less than this value, than the airfoil is too short for reattachment to occur.⁸ The use of flow control devices has demonstrated the ability to overcome the effects of the separation that forms on the upper surface of airfoils. There have been vast efforts to implement flow control by means of controlling the boundary layer. Some of the devices tested include

*Graduate Student; Student Member AIAA; dareas0@engr.uky.edu.

†Assistant Professor; Associate Fellow AIAA; rplebeau@engr.uky.edu.

Copyright © 2007 by the authors. Published by the American Institute of Aeronautics and Astronautics, Inc. with permission.

synthetic jets, plasma actuators and morphing wings.^{10–12} The “bumps” on the upper and lower surfaces of wings serve as a passive flow control device that has demonstrated the ability to reduce the amount of separation above the upper surface by means of tripping the flow. Traditional surface roughness typically increases the L/D or C_l/C_d ratio at low Reynolds numbers, but is detrimental at higher Reynolds numbers.⁸ However, the effect of the “bumps” is a fundamentally different phenomenon. The aerodynamic effects due to the bumps on the surface of these wings has been shown to be favorable in terms of wing performance at Reynolds numbers of $\mathcal{O}10,000$.⁹ Thus far, one wing profile has been investigated experimentally and numerically. The profile is based on the Eppler 398 profile and consists of bumps that have a radius $\approx 2\%c$. The effects due to the “bumps”, not clearly understood thus far, prompted numerical investigation.

Flight in atmospheres such as those encountered on Mars is characterized by relatively high flight speeds at relatively low Reynolds numbers approaching transonic conditions. These types of flight regimes can inhibit a drastic decrease in lift and and dramatic increase in drag.¹³ For air at extreme altitudes the mean free path can be rather large; thus, the no-slip condition is many times invalid and boundary layer phenomena as we know it is also invalid.¹⁴ Thus, all numerical simulations are assumed to simulate low Reynolds number flight regimes typical of UAVs and not necessarily flight regimes typical of near space space flight on Earth or that in the Martian atmosphere.

A. Motivation for Numerical Investigation

Smoke-wire flow visualization as described in Batill and Mueller¹⁵ was used for qualitative observation of the separation region on the upper surface of airfoils. A wire doped with model train smoke mixture and placed in front of the wing. Introducing a current to this wire heats the smoke mixture making smoke trails around the wing. A video camera and frame-grabber system were used to capture images. Details of the experimental setup can be found elsewhere.⁹

Of initial interest was whether the inflatable-rigidizable wing profile,¹⁶ including a blunt trailing edge, required a smooth “skin” over the bumpy surface and the addition of a sharper trailing edge. At low Re , as seen in Figure 1, the surface perturbations on the bumpy E398 wing actually improve the flow over the wing compared to the smooth wing by reducing the separation region for $Re = 25,000$ with α of 0° . Note that flow stream lines above the trailing edge are not distinct in some images due to the transition region disruption. One result of the flow visualization was the decision to forgo adding a smooth skin or sharp trailing edge to the inflatable-rigidizable wing design. However, thorough experimental results have not been obtained for lift and drag data, but the smoke-wire visualization reveals that the flow over the bumpy profiles is less separated than that of the smooth airfoils at Reynolds numbers on $\mathcal{O}10,000$.

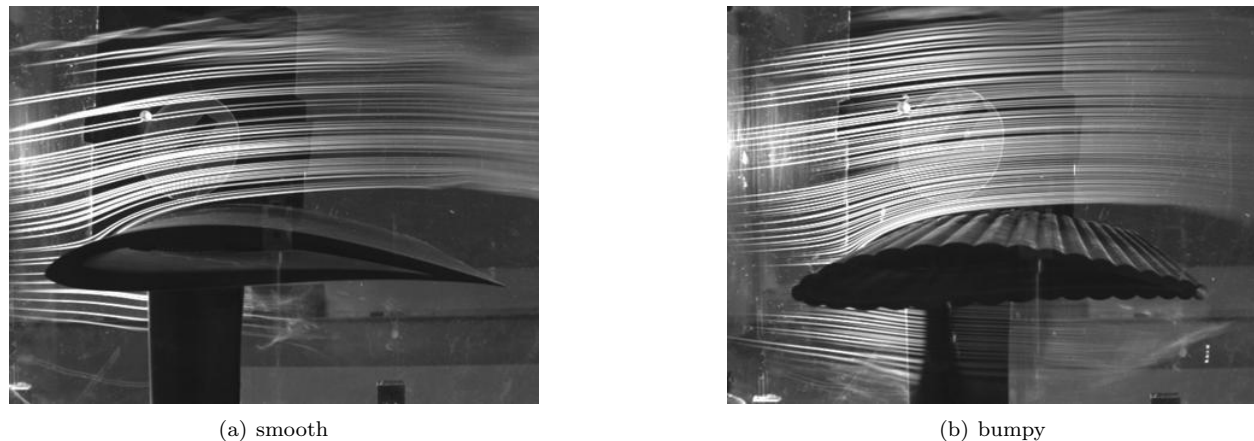


Figure 1. Smoke-wire flow visualization of Eppler 398 airfoil for $Re = 25k$, $\alpha = 0^\circ$

II. Computational Tools and Resources

A. UNCLE

Two in-house computational fluid dynamics (CFD) codes are used for the numerical investigation of the effects of the bumps on airfoils. The first code used is UNCLE, which was originally written by P.G. Huang.

It is a two/three-dimensional, finite-volume, unstructured incompressible Navier-Stokes solver for steady and unsteady flows. It relies on a cell-centered pressure-based method based on the SIMPLE algorithm with second order accuracy in both time and space. In order to compute numerical flux on interfaces, a second order upwind scheme is adopted to compute advection terms and second order centered difference scheme is used for diffusion terms. A collocated grid system with the Rhie and Chow¹⁷ momentum interpolation method¹⁸ is employed to avoid the checkerboard solution of the pressure based scheme. Fluxes on the volume faces are determined through interpolation of cell-centered values. The time discretization is a second-order fully implicit scheme. The version of UNCLE used to generate the results seen in the following section implements two Reynolds-Averaged Navier-Stokes (RANS) models including the one-equation Spalart-Allmaras¹⁹(SA) and the two-equation Shear Stress Transport²⁰(SST) turbulence models. Being unstructured in nature, UNCLE utilizes a Gauss-Seidel point solver for solving the flow field properties.

B. GHOST

The second CFD code used is titled GHOST, also originally written by P.G. Huang. It is a structured two-dimensional, finite-volume, incompressible Navier-Stokes solver for steady and unsteady flows. This code makes use of the SA turbulence model. The QUICK scheme is applied to discretize the advection terms with second order accuracy. A second order centered difference scheme is used for the diffusion terms. For the SA turbulence model, the Total Variation Diminishing (TVD) scheme is used for the advection terms. The time discretization is second order upwind and uses the delta-form sub-iterative scheme. This code has also undergone vast optimization techniques for minimizing memory usage and L2 cache misses. Being a second order structured grid code, its solver is based on the Thomas Algorithm (TDMA) solver. GHOST also includes the Suzen-Huang Transition model.²¹ GHOST also has the capability to use overset grids. Both UNCLE and GHOST are written in FORTRAN90 and include the capabilities to utilize MPI parallel computing on both 32-bit and 64-bit architectures.

C. Computing Resources

The results presented herein were obtained through the use of Kentucky Fluid Cluster 3 (KFC3) which employs 32 Pentium 4 2.4Ghz nodes, KFC4 which contains 48 AMD Athlon XP 2500+ processors, KFC5 which contains 47 AMD Athlon 64 3200+ processors, and KFC6 which contains 23 AMD Athlon 64x2 4600+ processors and 24 Intel Core 2 Duo e6400 processors.

III. Grid Resolution Study

The Eppler 398 “bumpy” profile is based on the bumps seen within the “smooth” profile in Figure 2. The unstructured grids used with UNCLE are generated with the commercial grid generation software GambitTM. An example of one of the grids generated is seen in Figure 3. Once the grid is generated in Gambit, an in-house partition program that includes the partitioning algorithm from METIS²² is used to break the mesh for parallel computing and to obtain proper node balancing for computing efficiency. For the structured grids used with GHOST and in-house C++/FORTRAN90 program is used to generate the grids. An example of one such grid can be seen in Figure 4.

All grids constructed, both structured and unstructured were made to achieve a dimensionless y spacing $y^+ \equiv \frac{u\tau y}{\nu} \sim 1$. Generating grids that ensure a $y^+ \sim 1$ is essential to guarantee that the grid used has an adequate number of grid points within the viscous sublayer region of the boundary layer. The grid spacings in the y direction were typically on the $\mathcal{O}10^{-5}$. For the bumpy airfoils it is also essential to achieve an adequate x grid spacing such that the intricate flow within the crevices between the bumps is captured. This study concluded that an x grid point spacing needs to exceed 30 divisions/bump to capture the vorticity, pressure, and velocity in the vicinity of the bumps accurately.

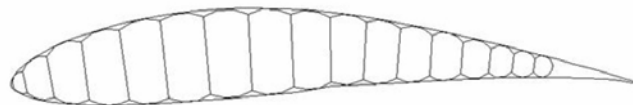
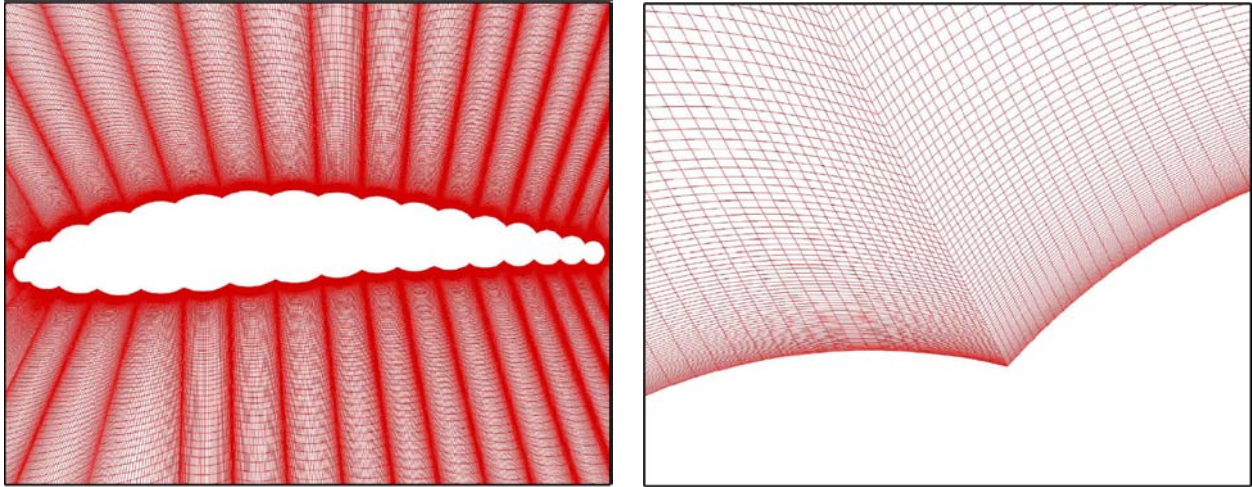


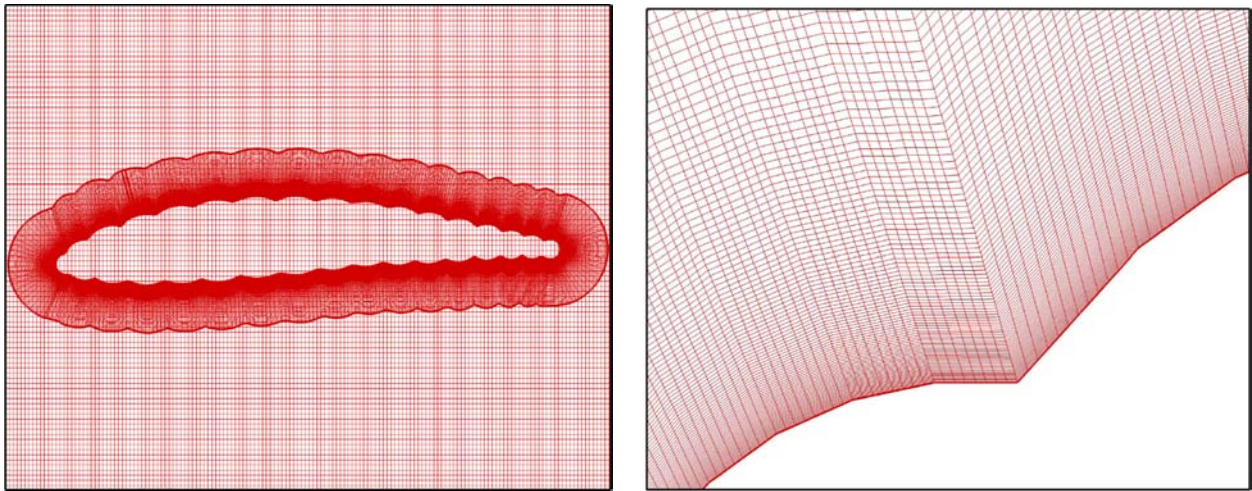
Figure 2. Modified Eppler 398 profile demonstrating the “bumpy” profile within the “smooth” profile.



(a) full

(b) zoomed

Figure 3. Unstructured grid used in UNCLE with $\sim 300,000$ grid points.



(a) full

(b) zoomed

Figure 4. Structured grid used in GHOST with $\sim 300,000$ grid points.

Not only were there resolution studies pertaining to the number of divisions per bump, but there was also an investigation into whether or not blocking was an issue with the smaller structured grids.

IV. Results

The test cases are summarized in Table 1. The free stream turbulence intensity (FSTI) is assumed to be 1% of the free stream velocity magnitude for all test cases ran. One limitation of using UNCLE for this type of application is that it does not possess a transition model which could be helpful to more accurately predict results for the flow over the “bumpy” airfoils. Further simulations with the Suzen-Huang transition model will be ran with GHOST. The cases corresponding to $Re = 18k$ and $Re = 36k$ were initially presented at the 45th AIAA Aerospace Sciences Meeting and Exhibit in Reno, NV.²³ The results for $Re = 25k$ are new for this paper and further analysis for each of the previously discussed cases has also been included.

Table 1. Test Cases

Airfoil	Re	α	Bumpy	Ideal
E398	18k	$7^\circ, 10^\circ$	-	✓
E398	18k	$7^\circ, 10^\circ$	✓	-
E398	36k	$7^\circ, 10^\circ$	-	✓
E398	36k	$7^\circ, 10^\circ$	✓	-
E398	25k	0°	-	✓
E398	25k	0°	✓	-

For the analysis presented herein we will make use of several non-dimensional quantities. The following is a summary of those used to avoid ambiguity. The static pressure is non-dimensionalized as $p^* = (p - p_\infty) / \rho U_\infty^2$. The x component of velocity is non-dimensionalized with the freestream velocity (e.g. $u^* = U_x / U_\infty$). Time is non-dimensionalized with the velocity and chord length (e.g. $t^* = (U_\infty t) / c$). The x and y coordinate length scales are non-dimensionalized with the chord length (e.g. $x^* = x / c$, $y^* = y / c$).

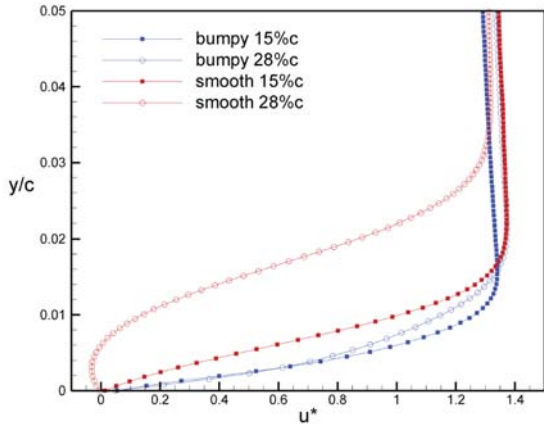
A. Velocity Profiles

The effects that the large scale surface roughness or “bumps” can be grasped more quantitatively through analysis of the velocity profiles normal to the surface at different chord locations. To make the analysis more consistent, the velocity profiles are extracted normal to the upper surface of both types of airfoil and the chord locations are chosen such that none of the profiles are extracted in the crevices between the bumps, but rather on the highest point of the bumps. The analysis done on the velocity profiles is done for both Eppler 398 profiles for the range of Reynolds numbers and angles of attacks mentioned previously. The purpose of this investigation is to increase the understanding of the separation control mechanism associated with the “bumps” on the upper and lower surfaces of the bumpy airfoil.

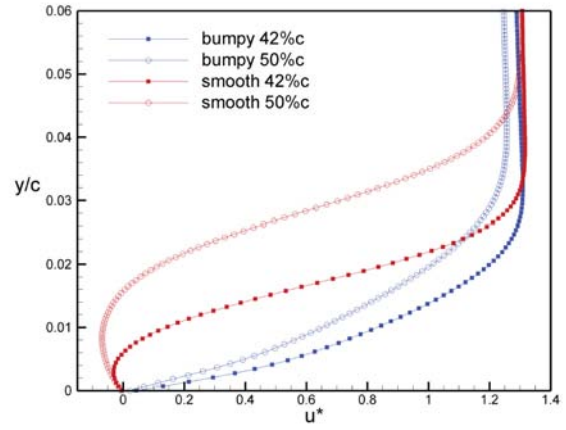
In Figure 5 the bumpy profile promotes a thinner boundary layer than that of the smooth airfoil at both chord locations near the leading edge. However, at $15\%c$ the difference between the boundary layer thickness for the bumpy and smooth profiles is much less than that at $28\%c$. The definite reason is unknown, but one possibility is the improvement downstream of the leading edge is more significant because the flow is tripped by more of the bumps than the location closer to the leading edge. Velocity profiles even further downstream at $42\%c$ and $50\%c$ respectively show a distinct improvement in removing separation from the flow above the upper surface. As the Reynolds number is doubled from $18k$ to $36k$ the improvements of the “bumpy” profile over the “smooth” profile exhibited at $Re = 18k$ is somewhat diminished. In fact, at $15\%c$ the smooth airfoil actually demonstrates a thinner boundary layer than that of the bumpy profile. At $28\%c$ the slope of the velocity with respect to the distance from the upper surface is fundamentally different, but the thickness of the boundary layer is comparable. Also, at $Re = 36k$, the maximum velocity at the respective chord locations is actually less for the bumpy airfoil than that of the smooth airfoil. This loss in dynamic pressure is assumed to be due to the addition of the bumps. This ultimately leads to a decrease in C_p and a decrease in lift (see Table 2).

B. Comments on Pressure

The amount of lift and drag generated by an airfoil is directly influenced by the coefficient of pressure on the upper and lower surfaces. We express the coefficient of pressure as $C_p = (p - p_\infty) / (\frac{1}{2} \rho U_\infty^2)$ where the maximum value will be unity on the leading edge of the airfoil, at the stagnation point. In Figure 7 a plot

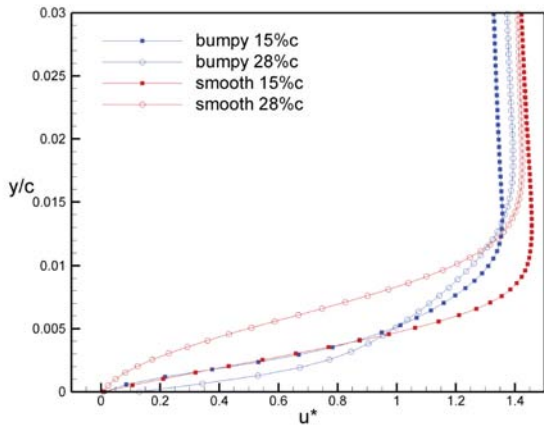


(a) 15%c and 28%c

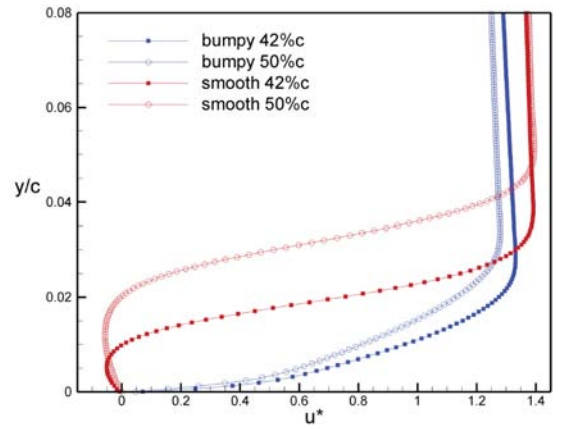


(b) 42%c and 50%c

Figure 5. Time averaged velocity profiles $Re = 18k$, $\alpha = 7^\circ$.



(a) 15%c and 28%c



(b) 42%c and 50%c

Figure 6. Time averaged velocity profiles for $Re = 36k$, $\alpha = 7^\circ$.

Table 2. Lift, drag and Strouhal number results.

Airfoil	Re	α	C_l	ΔC_l	C_d	ΔC_d	L/D	St
E398 smooth	18k	7°	1.041	0.481	0.012	0.025	86.59	1.4
E398 bumpy	18k	7°	0.657	0.041	0.021	0.002	31.56	3.4
E398 smooth	18k	10°	1.232	0.468	0.040	0.051	29.72	1.4
E398 bumpy	18k	10°	0.819	0.148	0.069	0.007	11.88	3.4
E398 smooth	36k	7°	1.316	0.587	0.040	0.040	33.19	1.4
E398 bumpy	36k	7°	0.690	0.288	0.028	0.012	24.46	3.4
E398 smooth	36k	10°	1.287	-	0.099	-	12.94	1.2
E398 bumpy	36k	10°	0.873	0.348	0.082	0.017	10.70	3.4
E398 smooth	25k	0°	0.236	0.260	0.057	0.019	4.09	2.2
E398 bumpy	25k	0°	0.522	0.950	0.0469	0.194	11.15	1.4

of the pressure coefficient vs. dimensionless length, x^* , is presented. The bumpy profile length is slightly less than one; this is consistent with Figure 2. Figure 7 demonstrates the fact that the pressure coefficient associated with the “bumpy” profile varies within each of the bumps. This figure also demonstrates that there is a dynamic pressure loss that is assumed to be due to the bumps and significantly reduces the area enclosed by the C_p curve. The lift results presented in Table 2 show that the amount of lift associated with the ideal profile is greater than the bumpy profile for this test case, which is consistent with Figure 7. The difference between the C_p curves at the lower Reynolds number is less than that at the higher Reynolds number. The difference in lift seen in Table 2 is also more for $Re = 36k$ ($\Delta C_l \approx .63$) than for $Re = 18k$ ($\Delta C_l \approx .38$). The large spikes seen in the C_p curve for the smooth airfoil is due to the vortex shedding off the trailing edge of the airfoil. The evolution of the spike in this region can be seen by looking at a series of instantaneous plots. In Figure 7b the spike in the C_p curve is more pronounced. The size and intensity of the vortices being shed at $Re = 36k$ were observed to be greater than that at the lower Reynolds numbers. The presence of the bumps seen in the pressure coefficient plot is diminished near the location on the upper surface where the vortex shedding occurs. It was also observed in coarse grids that the presence of the bumps was not captured adequately in the C_p plot until resolution in x spacing was increased.

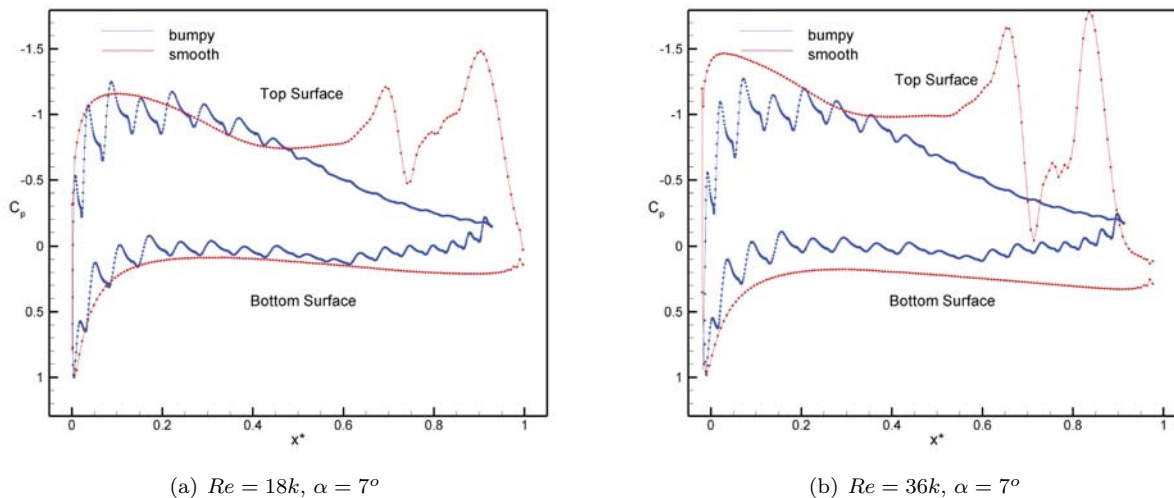


Figure 7. Time averaged C_p vs. x^* plot.

C. Lift Variation

The flow over the airfoils discussed herein is inherently unsteady. Experimental literature suggests that the flow over the “smooth” airfoils is more steady than that over the “bumpy” airfoils.⁹ Unsteady flow is commonly characterized by the Strouhal Number, $St = (fL)/(U_\infty)$. The frequency is the reciprocal of the period of vortex shedding and the characteristic length is the chord length in the cases presented thus far. The frequency of vortex shedding was taken to be approximately the fundamental frequency of the lift coefficient. Fast Fourier Analysis (FFT) was done on the variation of the lift coefficient with respect to t^* to obtain the fundamental frequencies for these test cases. The results for the Strouhal Numbers are given in Table 2. Numerical results are consistent with the experimental observation⁹ that the flow over the “smooth” airfoil was steadier than the flow over the “bumpy” airfoils. The frequency observed for the “bumpy” Eppler profile was more than double that of the “smooth” Eppler profile in the cases with $\alpha \neq 0^\circ$. When $\alpha = 0^\circ$, then the frequencies observed are different in that the fundamental frequency for the smooth airfoil is increased which is consistent with previous observations for Low Reynolds number flow over airfoils.²⁴ The frequency associated with the bumpy airfoil is decreased. The precise reason is unknown, but the frequency of vortex shedding is consistent with the results seen in Figure 8. It should also be noted that when the lift reaches a value less than zero in these C_l oscillations an overlap in the upper and lower surfaces in the C_p curve is observed.

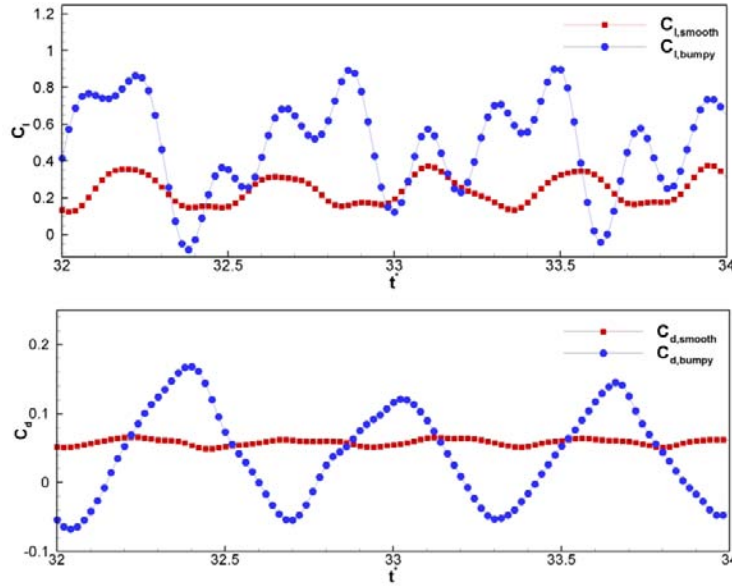


Figure 8. Lift and drag variation plotted against t^* for $Re=25k$, $\alpha = 0^\circ$.

D. Vorticity

In Figure 9 more detail is shown in the vicinity of the bumps for $Re = 18k$, $\alpha = 7^\circ$. Here it is clear that within each of the bumps vortices form. This formation of the vortices is assumed to be the fundamental mechanism that prevents the separation seen in the “smooth” airfoil simulations. However, in Table 2 we can see that the lack of separation does not necessarily mean that the amount of lift will increase. The separation associated with smooth airfoils at relatively low Reynolds numbers is fundamentally different than that observed for Reynolds numbers of $\mathcal{O}10^6$. The difference between the separation regions is that at high Reynolds numbers the separation region typically consists of stagnant flow whereas in the low Reynolds number regime the separation is analogous with vortex shedding on the upper surface. The observed vortices between the bumps on the upper surfaces of the airfoils have streamlines in the clockwise direction whereas the vortices between the bumps on the bottom surface have streamlines in the counter-clockwise direction. Figure 10 displays the vortex formations for the smooth airfoil and Figure 11 displays the vortex formations for the bumpy airfoil. The vorticity contours reveal that although the streamlines indicate that there is circulation within the crevices, the strength of the vorticity associated with that circulation is relatively weak compared to the fundamental vortex shedding of the airfoil itself. In previous studies^{25–27} the shedding of vortices from the smooth airfoils is also seen at these low Reynolds numbers.

As mentioned previously, there is critical value for the Reynold number for smooth airfoils for which a laminar boundary layer can reattach. Since the simulations presented herein are below this specific value we would expect the boundary layers not to reattach in our simulations. The phenomenon of vortex shedding from the upper surface without reattachment is consistent with previously documented studies. However, by looking at a sequence of vorticity plots one can see that the boundary layer tries to reattach, but lacks adequate length to do so. If the airfoils were slightly larger, large enough to increase the chord based Reynolds number to that of $\approx 70,000$, then we would expect to see the laminar boundary layer to reattach. If the boundary layer reattaches than the fundamental frequency of vortex shedding and the frequency of oscillations in the lift and drag would also change.

The vortex phenomena observed is similar to that seen in dynamic stall studies. In dynamic stall the flowfield near an airfoil undergoes a pitching motion causing a primary vortex to form above the upper surface of the airfoil. While this vortex is present above the upper surface a dramatic increase in lift is observed. When the vortex sheds into the wake of the airfoil stall occurs resulting in a dramatic decrease in lift.²⁸ This type of phenomenon is consistent with the oscillations observed in the lift and drag seen in Figure 8. In Figures 10,11 we can see further evidence that as the vortex forms over the upper surface of the airfoil the lift is at its local minimum for the particular period of the C_l oscillation. For the bumpy airfoil, we see that the vortex formations are more complicated and the oscillations in C_l reflect that characteristic

of the flowfield.

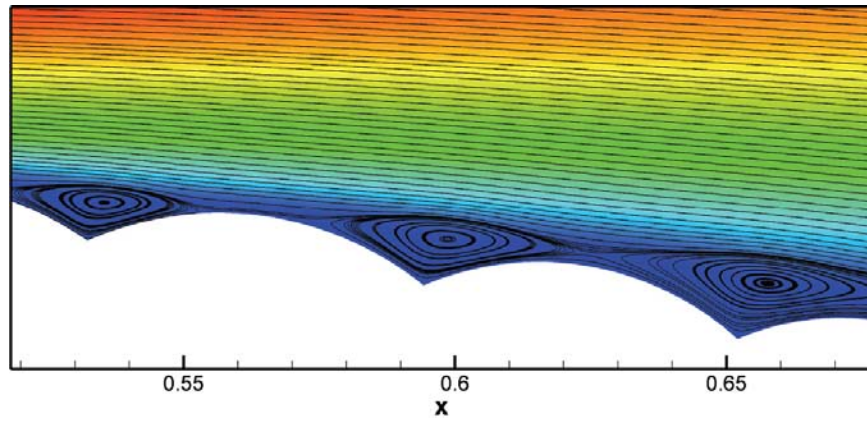


Figure 9. Streamlines over the top surface of E398 bumpy airfoil for $Re = 18k$, $\alpha = 7^\circ$ with u^* velocity contour.

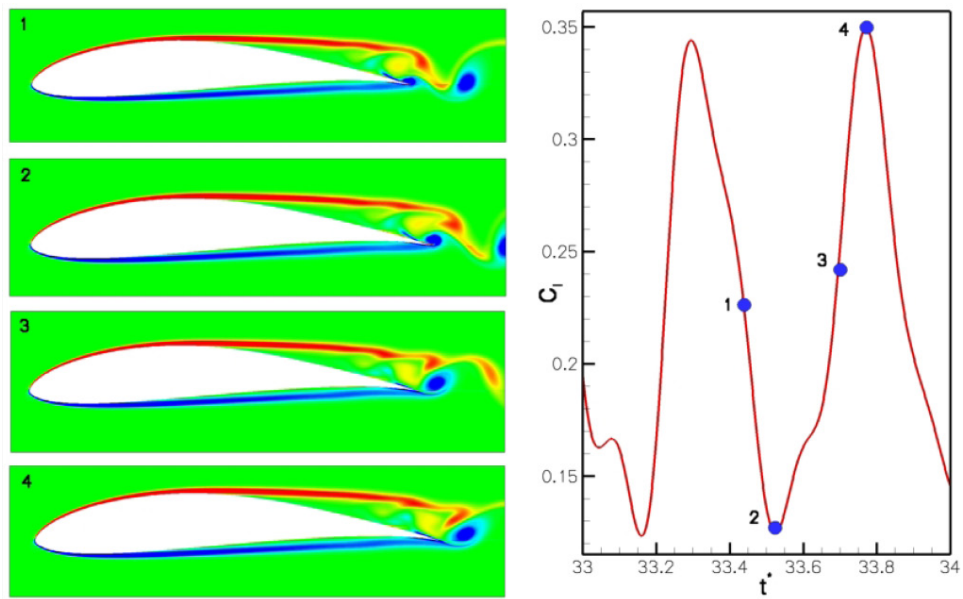


Figure 10. Instantaneous vorticity contours for smooth E398 airfoil at $Re = 25k$, $\alpha = 0^\circ$.

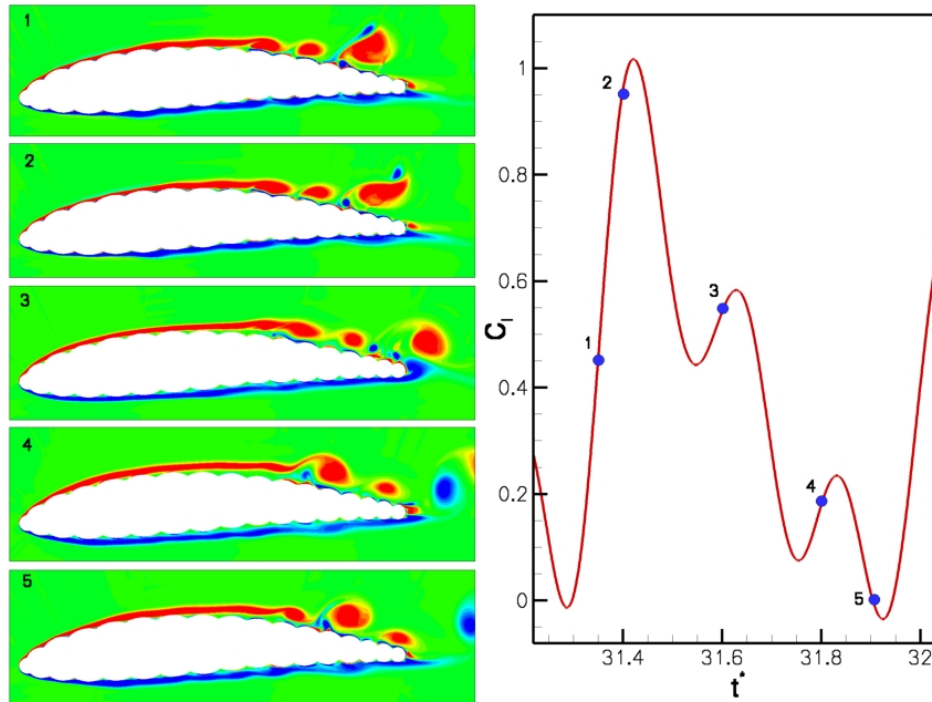


Figure 11. Instantaneous vorticity contours for bumpy E398 airfoil at $Re = 25k$, $\alpha = 0^\circ$.

V. Summary and Future Work

Experimental observations suggested that the flow over the “bumpy” Eppler 398 profile was more attached than that over the “smooth” Eppler 398 airfoil at relatively low Reynolds numbers. In addition, the flow over the “bumpy” profile was observed to exhibit more unsteadiness. Numerical simulations were carried out to further investigate the effects of the bumps on the flow over the airfoil. The results are consistent with experimental observations that the flow over the bumpy airfoil has less separation than that over the smooth profile. However, numerical results suggest that there is a large amount of unsteadiness related to the lift and drag coefficients and this is due to the vortex shedding phenomena seen at these low Reynolds numbers.

Due to the vast number of geometries that can be constructed using bumpy profiles there are ongoing simulations that wish to determine the optimum configuration for a given application. Through the use of data obtained from a large number of simulations the optimum configuration for bump height, bump radius, and the number of bumps needs to be determined. Since the baseline profile for bumpy airfoil configurations does not coincide with common smooth airfoils used in the same flight regime, the complexity of the process to determine the ideal configuration invites a thorough investigation. To do so, adequate experimental data needs to be obtained for various airfoil configurations at various angles of attack and Reynolds numbers. Also, there is interest from individuals at ILC Dover to investigate the effects that a smooth trailing edge can have on the performance of the bumpy wings at these low Reynolds number flight regimes.

Acknowledgments

The authors would like to acknowledge ILC Dover and the Kentucky Space Grant Consortium for making inflatable wings available to the University of Kentucky and for funding this research. This work is also supported by NASA Glenn Research Center through the use of KFC3.

References

- ¹Simpson, A., Jacob, J., Smith, S., "Flight Control of a UAV with Inflatable Wings with Wing Warping," AIAA Paper 2006-2831, 24th AIAA Applied Aerodynamics Conference, San Francisco, California, June 5-8, 2006.
- ²Kenney, P., Croon, M., "Simulating the Ares Aircraft in the Mars Environment," AIAA Paper 2003-6579, 2nd AIAA "Unmanned Unlimited" Conf. and Workshop and Exhibit, San Diego, California, Sep. 15-18, 2003.
- ³Guynn, M.D., Croon, M.A., Smith, S.C., Parks, R.W., Gelhausen, P.A., "Evolution of a Mars Airplane Concept for the Ares Mars Scout Mission," AIAA Paper 2003-6578, 2nd AIAA Unmanned Unlimited Systems, Technologies, and Operations - Aerospace, San Diego, CA, September 15-18, 2003.
- ⁴Lede, J., Parks, R., "High Altitude Drop Testing in Mars Relevant Conditions for the ARES Mars Scout Mission," AIAA Paper 2003-6609, 2nd AIAA "Unmanned Unlimited" Conf. and Workshop and Exhibit, San Diego, California, Sep. 15-18, 2003.
- ⁵Lafleur, J., Olds, J., Braun, R., "Daedalon: A Revolutionary Morphing Spacecraft Design for Planetary Exploration," AIAA Paper 2005-2771, 1st Space Exploration Conference: Continuing the Voyage of Discovery, Orlando, FL, Jan. 30 - Feb. 1, 2005.
- ⁶Cadogan, D., Smith, T., Uhelsky, F., MacKusick, M., "Morphing Inflatable Wing Development for Compact Package Unmanned Aerial Vehicles," AIAA Paper 2004-1807, 45th AIAA/ASME/ASCE/AHS/ASC Structures, Structural Dynamics and Materials Conference, Palm Springs, CA, Apr. 19-22, 2004.
- ⁷Simpson, A., Jacob, J., "Aerodynamic Control of an Inflatable Wing Using Wing Warping," AIAA Paper 2005-5133, 35th AIAA Fluid Dynamics Conference and Exhibit, Toronto, Ontario, June 6-9, 2005.
- ⁸Lissaman, P.B.S., "Low-Reynolds-Number Airfoils", Annual Review of Fluid Mechanics, Volume 15, pp.223-239, 1983.
- ⁹Santhanakrishnan, A., Jacob, J., "Effect of Regular Surface Perturbations on Flow Over an Airfoil," AIAA Paper 2005-5145, 35th AIAA Fluid Dynamics Conference & Exhibit, Ontario, June 6-9 2005.
- ¹⁰Santhanakrishnan, A., Jacob, J., "Flow Control Using Plasma Actuators and Linear/Annular Plasma Synthetic Jet Actuators," AIAA Paper 2006-3033, 3rd AIAA Flow Control Conference, San Francisco, CA, June 2006.
- ¹¹Vorobiev, A., Rennie, R., Jumper, E., "An Experimental Investigation of Lift Enhancement and Roll Control Using Plasma Actuators," AIAA Paper 2006-3383, 37th AIAA Plasmadynamics and Lasers Conference, San Francisco, California, June 5-8, 2006.
- ¹²Santhanakrishnan, A., Pern, N., Ramakumar, K., Jacob, J., "Enabling Flow Control Technology for Low Speed UAVs," AIAA Paper 2005-6960, Infotech@Aerospace, Arlington, Virginia, Sep. 26-29, 2005.
- ¹³Guynn, M.D., Croom, M.D., Smith, S.C., Parks, R.W., Gelhausen, P.A., "Evolution of a Mars Airplane Concept for the Ares Mars Scout Mission," AIAA Paper 2003-6578, 2nd AIAA "Unmanned Unlimited" Systems Technologies, and Operations, San Diego, CA, Sept. 2003.
- ¹⁴Abbott, I.H., Von Doenhoff, A.E., *Theory of Wing Sections*, Dover Publications, Mineola, NY, 1959.
- ¹⁵Batill, S., Mueller, T. "Visualization of Transition in the Flow Over an Airfoil Using the SmokeWire Technique," AIAA Journal, Vol. 19, pp. 340-345, 1981.
- ¹⁶Cadogan, D., Graham, W., Smith, T., "Inflatable and Rigidizable Wings for Unmanned Aerial Vehicles", AIAA Paper 2003-6630, 2nd AIAA "Unmanned Unlimited" Conf. and Workshop and Exhibit, San Diego, California, Sep. 15-18, 2003.
- ¹⁷Rhie, C.M., Chow, W.L., "Numerical study of the turbulent flow past an airfoil with trailing edge separation," AIAA Journal, Vol. 21, 1983, pp. 1525-1532.
- ¹⁸Chen, H., Huang, P.G., LeBeau, R.P., "A Cell-Centered Pressure Based Method for Two/Three-Dimensional Unstructured Incompressible Navier-Stokes Solver," AIAA-2005-0880, 2005.
- ¹⁹Spalart, P.R., Allmaras, S.R., "A One-Equation Turbulence Model for Aerodynamic Flows," AIAA Paper 92-0439, 1992.
- ²⁰Menter, F.R., "Zonal Two Equation κ - ω Turbulence Models for Aerodynamic Flows," AIAA Paper 93-2906, 1993.
- ²¹Suzen, Y.B., Huang, P.G., "Modeling of Flow Transition Using an Intermittency Transport Equation," Journal of Fluids Engineering, Volume 122, pp. 273-284, 2000.
- ²²Karypis, G., Kumar, V., "A software package for partitioning unstructured graphs, partitioning meshes, and computing fill-reducing ordering of sparse matrices," Version 4.0, 1998.
- ²³Reasor, D.A., LeBeau, R.P., Smith, S.W., Jacob, J.D., "Flight Testing and Simulation of a Mars Aircraft Design Using Inflatable Wings," 45th AIAA Aerospace Sciences Meeting and Exhibit, AIAA Paper 2007-0243, Reno, NV, 2007.
- ²⁴Katam, V., "Simulation of Low-Re Flow over a modified NACA 4415 Airfoil with Oscillating Chamber," Master's Thesis, Dept. of Mechanical Engineering, University of Kentucky, 2005.
- ²⁵Katam, V., LeBeau, R.P., Jacob, J.D., "Experimental and Computational Investigation of a Modified NACA 4415 in Low-Re Flows," 22nd Applied Aerodynamics Conference and Exhibit, AIAA-2004-4972, Providence, RI, August 16-19, 2004.
- ²⁶Katam, V., LeBeau, R.P., Jacob, J.D., "Simulation of Separation Control on a Morphing Wing with Conformal Camber," 35th AIAA Fluid Dynamics Conference and Exhibit, Toronto, Canada, July 6-9, 2005.
- ²⁷Pern, N.J., LeBeau, R.P., Jacob, J.D., "Characterization of Zero Mass Flux Flow Control for Low Speed Airfoil Separation Control: Adaptive Airfoil," AIAA-2006-3032, 3rd AIAA Flow Control Conference, San Francisco, CA, June 5-8, 2006.
- ²⁸Doligalski, T.L., Smith, C.R., Walker, J.D.A., "Vortex Interactions with Walls," Annual Review of Fluid Mechanics, Volume 26, pp. 573-616, 1994.